Int. J. Solids Structures Vol. 28, No. 3, pp. 329–339, 1991
Printed in Great Britain.

0020–7683/91 $3.00 + .00

THE STRESSES AROUND A PARTLY MICROCRACKED HOLE IN CERTAIN CERAMIC MATERIALS UNDER INTERNAL PRESSURE

A. E. GIANNAKOPOULOS and P. GUDMUNDSON
Department of Strength of Materials and Solid Mechanics, The Royal Institute of Technology, S-100 44 Stockholm, Sweden

(*Received* 2 *December* 1989; *in revised form* 27 *October* 1990)

Abstract—In the present work we examine the stress field around a hole in certain ceramic materials. The hole is under internal pressure in plane strain conditions. The material behavior is initially isotropic linearly elastic and upon loading develops microcracks. The damage is assumed to be anisotropic and microcracking is believed to take place along preferred orientations. A damaged constitutive law, appropriate for the microcracking assumptions, is used to derive exact results for the stress fields in this particular problem. The present analysis may find applications in the experimental investigation of ceramic materials behaving as anisotropically microcracking solids.

1. INTRODUCTION

A growing body of research is presently concerned with the development of mechanics of brittle solids such as ceramics. These are materials which while not undergoing plastic deformations of any significance at low temperatures, can nevertheless behave quite inelastically as a result of the nucleation of microcracks.

Ceramics are processed at high temperatures and then cooled to ambient. This causes single-phase ceramics to microcrack along the grain boundaries due to some external stress. Microcracks in these ceramic materials are typically isolated due to residual stress distributions and the inclined adjacent boundary facets (Fu, 1983). When tensile stress is applied to ceramics, favorably oriented grain boundary facets will crack. As the stress is raised, more grain facets crack and so stress-induced damage progresses with increasing applied tensile stress.

Consider a macroscopic element of the material. As the number of microcracks in the material increases, the material becomes more compliant. Anisotropy will develop because the maximum principal stress will influence the microcrack orientation. If the applied stress is removed after reaching a peak value, the microcracked density is retained since microcracking is an irreversible process. Therefore, the unloading stress–strain curve is linear, resulting in a hysteresis loop. The amount of strain energy dissipation is equivalent to the area enclosed by this hysteresis loop. We will assume that both the size of the microcracks and their separation are small and therefore a typical material element can be regarded as containing numerous microcracks (smeared damage) so that computations can be based on the effective behavior of the homogenized solid. The uniaxial stress–strain behavior of the material for this type of material is shown in Fig. 1a. This behavior will be simplified by assuming a trilinear stress–strain idealization, shown in Fig. 1b.

Assuming monotonic stress paths, a deformation theory of damage can be obtained. The stress–strain relation, provided that the material is initially uncracked, becomes (Ortiz, 1987; Ortiz and Giannakopoulos, 1989)

$$\varepsilon_{ij} = (C^0_{ijkl} + \lambda(\sigma_1) n_i n_j n_k n_l)\sigma_{kl} \tag{1}$$

where C^0_{ijkl} are the isotropic linearly elastic compliances of the uncracked material and $\mathbf{n}$ is

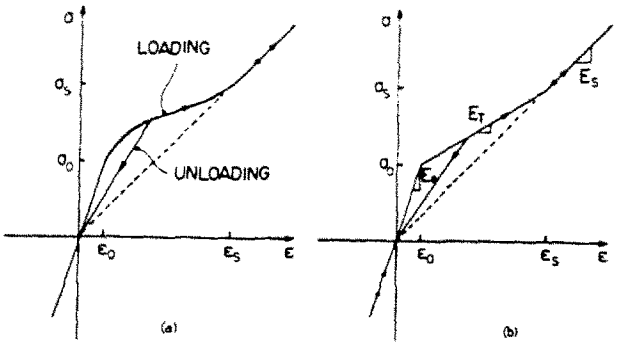

Fig. 1. (a) Elastic-damaged uniaxial behavior. (b) Assumed trilinear idealization of the uniaxial stress–strain curve.

the direction of maximum tensile stress σ_1. The function $\lambda(\sigma_1)$ is a measure of damage and from the trilinear uniaxial stress–strain law

$$\lambda(\sigma_1) = \begin{cases} 0, & \sigma_1 \leqslant \sigma_0 \quad (\sigma_0 > 0) \\ \left(\dfrac{1}{E_T} - \dfrac{1}{E_0}\right)\left(1 - \dfrac{\sigma_0}{\sigma_1}\right), & \sigma_0 \leqslant \sigma_1 \leqslant \sigma_s \\ \dfrac{1}{E_s} - \dfrac{1}{E_0}, & \sigma_s \leqslant \sigma_1. \end{cases} \tag{2}$$

Note that

$$E_T = \frac{\sigma_s - \sigma_0}{\varepsilon_s - \varepsilon_0}, \quad \varepsilon_0 = \frac{\sigma_0}{E_0} \quad \text{and} \quad \varepsilon_s = \frac{\sigma_s}{E_s}.$$

Equations (1) and (2) describe a nonlinear, anisotropic elastic material. There are three distinct regions of the stress–strain curve (Fig. 1b) which correspond to three possible microcracked stages of the material. In the elastic stage ($\sigma_1 \leqslant \sigma_0$), the material does not develop microcracking. In the saturation stage ($\sigma_1 \geqslant \sigma_s$), all possible microcrack sites are active and the material sustains no further damage. Between the elastic and the saturated region there is the transition zone ($\sigma_0 \leqslant \sigma_1 \leqslant \sigma_s$), where the material undergoes partial microcracking.

2. HOLE UNDER INTERNAL PRESSURE

The problem we will investigate is a hole of radius r_0 in an infinite ceramic medium that obeys eqns (1) and (2). At the faces of the hole we apply an internal pressure $p_0 \geqslant 0$ (Fig. 2). The conditions for the material are plane strain, axisymmetric. Then, the only nonzero strains will be ε_{rr} and $\varepsilon_{\theta\theta}$, with (r, θ) being the polar coordinates of the problem. From the elastic solution, we know that σ_{rr} and $\sigma_{\theta\theta}$ are the only nonzero stresses on the (r, θ) plane and they are also principal stresses.

If

$$p_0 \leqslant \sigma_0, \tag{3}$$

then the material behaves elastically and we have the well known elastic solution

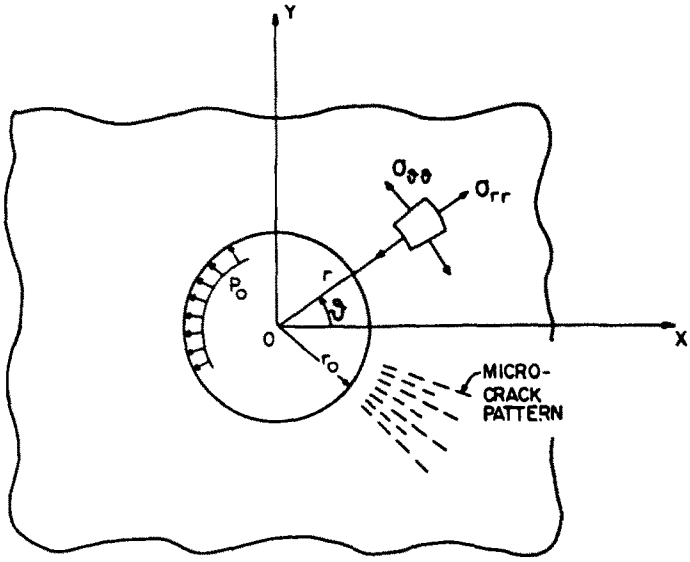

Fig. 2. Cylindrical hole of radius r_0 under internal pressure p_0.

$$\sigma_{rr} = -p_0\left(\frac{r_0}{r}\right)^2$$

$$\sigma_{\theta\theta} = p_0\left(\frac{r_0}{r}\right)^2$$

$$\sigma_{zz} = 0 \quad \text{for} \quad r \geqslant r_0. \tag{4}$$

Suppose we increase the applied pressure monotonically so that

$$p_0 > \sigma_0 > 0. \tag{5}$$

Then, microcracking will start forming in the vicinity of the hole. This microcracking will change the stress field around the hole. However, far enough from the hole eqn (4) will still hold, since the stresses decay rapidly. To proceed with the solution, we make the following assumptions which must be justified *a posteriori*:

$$\sigma_{\theta\theta} > \sigma_0$$
$$\sigma_{\theta\theta} > \sigma_{rr} \quad \text{for all} \quad r_0 \leqslant r. \tag{6}$$

The assumptions described by (6) simply state that $\sigma_{\theta\theta}$ is the maximum principal tensile stress at all times. Note that from the plane strain conditions ($\varepsilon_{zz} = 0$)

$$\sigma_{zz} = \nu_0(\sigma_{\theta\theta} + \sigma_{rr}) \tag{7}$$

and since the Poisson ratio of the intact material is limited by $-1 < \nu_0 < 1/2$, we conclude that $\sigma_{zz} < \sigma_{\theta\theta}$. The above assumption indicates that

$$\sigma_1 = \sigma_{\theta\theta}$$
$$\mathbf{n} = \begin{pmatrix} n_r \\ n_\theta \end{pmatrix} = \begin{pmatrix} 0 \\ 1 \end{pmatrix}. \tag{8}$$

Therefore, the microcracks will develop parallel to the radial directions, as shown in Fig. 2.

Then, the constitutive relations will have the following explicit form:

$$\varepsilon_{rr} = \frac{1-\nu_0^2}{E_0}\sigma_{rr} - \frac{(1+\nu_0)\nu_0}{E_0}\sigma_{\theta\theta}$$

$$\varepsilon_{\theta\theta} = -\frac{(1+\nu_0)\nu_0}{E_0}\sigma_{rr} + \left[\frac{1-\nu_0^2}{E_0} + \lambda(\sigma_{\theta\theta})\right]\sigma_{\theta\theta} \tag{9}$$

where $\lambda(\sigma_{\theta\theta})$ is given by eqn (2).

The only displacement entering the problem is the radial displacement $u_r(r)$. The geometric relations are then

$$\varepsilon_{\theta\theta} = \frac{u_r}{r}$$

$$\varepsilon_{rr} = \frac{\mathrm{d}u_r}{\mathrm{d}r}. \tag{10}$$

From eqn (10) we can write the compatibility equation for this problem as

$$\varepsilon_{rr} = \frac{\mathrm{d}}{\mathrm{d}r}(r\varepsilon_{\theta\theta}) = \varepsilon_{\theta\theta} + r\frac{\mathrm{d}\varepsilon_{\theta\theta}}{\mathrm{d}r}. \tag{11}$$

The equilibrium equation is simply

$$\sigma_{\theta\theta} = \frac{\mathrm{d}}{\mathrm{d}r}(r\sigma_{rr}). \tag{12}$$

We can write the stresses in terms of a potential, $X(r)$, so that equilibrium is automatically satisfied. Then

$$\sigma_{rr} = X(r)$$

$$\sigma_{\theta\theta} = X(r) + rX_{,r}(r). \tag{13}$$

Using eqns (13), (9) and (11) we may cast the governing equation for our problem as an ordinary differential equation in terms of $X(r)$:

$$r^2(A+\lambda)X_{,rr} + r(3A+3\lambda+r\lambda_{,r})X_{,r} + (\lambda+r\lambda_{,r})X = 0 \tag{14}$$

where

$$A = \frac{1-\nu_0^2}{E_0} > 0 \tag{15a}$$

$$\lambda = \begin{cases} 0; & \sigma_{\theta\theta} \leqslant \sigma_0 \\ \left(1 - \dfrac{\sigma_0}{X+rX_{,r}}\right)C = \left(1 - \dfrac{\sigma_0}{\sigma_{\theta\theta}}\right)C; & \sigma_0 \leqslant \sigma_{\theta\theta} \leqslant \sigma_s \\ D; & \sigma_s \leqslant \sigma_{\theta\theta} \end{cases} \tag{15b}$$

$$\lambda_{,r} = \begin{cases} 0; & \sigma_{\theta\theta} \leqslant \sigma_0 \\ \sigma_0 C\dfrac{2X_{,r}+rX_{,rr}}{(X+rX_{,r})^2}; & \sigma_0 \leqslant \sigma_{\theta\theta} \leqslant \sigma_s \\ 0; & \sigma_s \leqslant \sigma_{\theta\theta} \end{cases} \tag{15c}$$

$$C = \frac{1}{E_T} - \frac{1}{E_0} > 0 \tag{15d}$$

$$D = \frac{1}{E_s} - \frac{1}{E_0} > 0, \quad < C. \tag{15e}$$

The boundary conditions are

$$\left.\begin{aligned} &\sigma_{rr}(r = r_0) = -p_0 < 0 \\ &\left.\begin{matrix}\sigma_{rr} \\ \sigma_{\theta\theta}\end{matrix}\right\} \to 0, \quad r \to +\infty. \end{aligned}\right. \tag{16}$$

From continuity of tractions we have the following jump conditions for all $r > r_0$:

$$[\sigma_{rr}] = 0. \tag{17}$$

From continuity of displacements we have

$$[u_r] = 0. \tag{18}$$

From (18) and (10) we can assure that $[\varepsilon_{\theta\theta}] = 0$. Notice that $\lambda \cdot \sigma_{\theta\theta} = C(\sigma_{\theta\theta} - \sigma_0)$. Therefore, from eqn (9) we conclude

$$[\sigma_{\theta\theta}] = 0. \tag{19}$$

At the interfaces of the saturated, elastic and transition regions around the hole, $\sigma_{rr}(r = r_e) = -\sigma_0$, $\sigma_{\theta\theta}(r = r_e) = \sigma_0$, $\sigma_{\theta\theta}(r = r_s) = \sigma_s$, where r_e is the radius of the elastic boundary and r_s that of the saturation boundary (Fig. 3). Plane stress conditions can be easily obtained by changing ν_0 to $\nu_0/(1-\nu_0)$ and E_0 to $E_0/(1-\nu_0^2)$.

3. SOLUTION FOR THE STRESS FIELD

The general form of the solution of eqn (14) is given by the following expressions:

$$X = k_1^{\mathrm{I}} r^{-2} + k_2^{\mathrm{I}}; \quad \sigma_{\theta\theta} \leqslant \sigma_0 \tag{20a}$$

$$X = k_1^{\mathrm{II}} r^{-1+\xi_1} + k_2^{\mathrm{II}} r^{-1-\xi_1} + \sigma_0; \quad \sigma_0 \leqslant \sigma_{\theta\theta} \leqslant \sigma_s \tag{20b}$$

$$X = k_1^{\mathrm{III}} r^{-1+\xi_2} + k_2^{\mathrm{III}} r^{-1-\xi_2}; \quad \sigma_s \leqslant \sigma_{\theta\theta} \tag{20c}$$

$$\xi_1 = \left(\frac{A}{A+C}\right)^{1/2} \tag{20d}$$

$$\xi_2 = \left(\frac{A}{A+D}\right)^{1/2}. \tag{20e}$$

The constant coefficients $k_1^{\mathrm{I}}, k_2^{\mathrm{I}}, \ldots, k_3^{\mathrm{III}}$ will be determined from the boundary conditions on the hole face and at infinity, and from the continuity of tractions at the interfaces. Note that the general solution (20) may also be useful for solving the thick tube problem, by appropriately changing the boundary conditions.

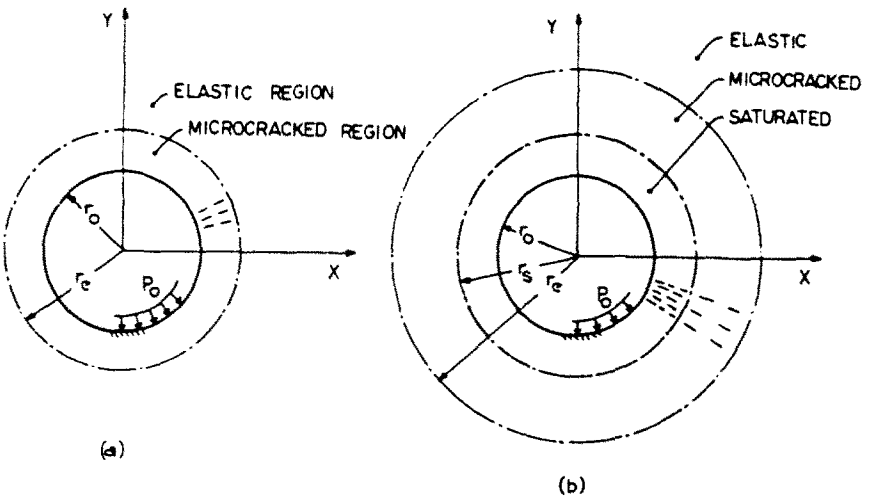

Fig. 3. The possible elastodamage boundaries for a hole under internal pressure p_0. (a) $\sigma_0 \leqslant p_0 \leqslant \sigma_s$; (b) $\sigma_s < p_0$.

To proceed with determining the constant coefficients, it is convenient to distinguish two cases. In the first case (Fig. 3a), there is an elastic region and a transition region, so that eqns (20a) and (20b) apply. In the second case (Fig. 3b), there is in addition a saturated region, meaning that eqn (20c) applies as well. The regions are separated by circular boundaries. We denote the boundary of the saturation region by r_s. Clearly

$$0 < r_0 < r_s < r_e.$$

The elastic solution will read as

$$\sigma_{rr}(r \geqslant r_e) = -\sigma_0\left(\frac{r_e}{r}\right)^2$$

$$\sigma_{\theta\theta}(r \geqslant r_e) = \sigma_0\left(\frac{r_e}{r}\right)^2. \tag{21}$$

For the transition region the solution will behave as

$$\sigma_{rr}(r_s \leqslant r \leqslant r_e) = c_1 r^{-1+\xi_1} + c_2 r^{-1-\xi_1} + \sigma_0$$
$$\sigma_{\theta\theta}(r_s \leqslant r \leqslant r_e) = \xi_1(c_1 r^{-1+\xi_1} - c_2 r^{-1-\xi_1}) + \sigma_0. \tag{22}$$

For the saturation region the solution will be

$$\sigma_{rr}(r_0 \leqslant r \leqslant r_s) = d_1 r^{-1+\xi_2} + d_2 r^{-1-\xi_2}$$
$$\sigma_{\theta\theta}(r_0 \leqslant r \leqslant r_s) = \xi_2(d_1 r^{-1+\xi_2} - d_2 r^{-1-\xi_2}). \tag{23}$$

The coefficients c_1 and c_2 can be determined from the continuity of stresses between the elastic and the transition distributions of stresses. The result is

$$c_1 = -\sigma_0 r_e^{1-\xi_1}$$
$$c_2 = -\sigma_0 r_e^{1+\xi_1}. \tag{24}$$

The coefficients d_1 and d_2 can be determined from continuity of stresses between the transition and the saturation distributions of stresses. The result is

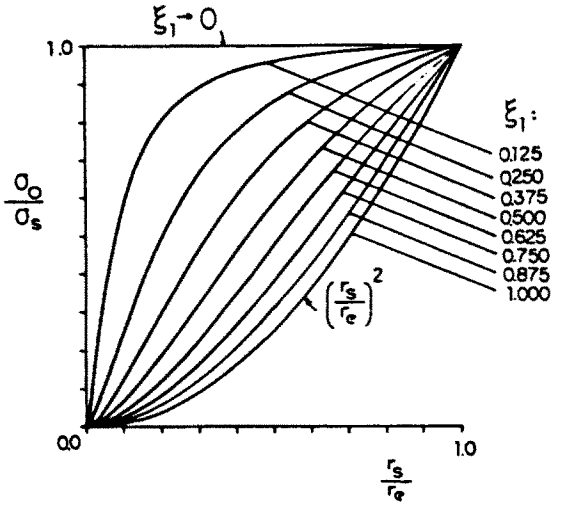

Fig. 4. The dependence of r_s/r_e on σ_0/σ_s for a hole under internal pressure.

$$\xi_1 = \left(\frac{E_r - \nu_0^2 E_T}{E_0 - \nu_0^2 E_T}\right)^{1/2}, \quad 0 < \xi_1 \leqslant 1.$$

$$d_1 = \frac{r_s^{1-\xi_2}}{2}\left[\sigma_0 + \frac{\sigma_0}{\xi_2} - \sigma_0\left(1+\frac{\xi_1}{\xi_2}\right)\left(\frac{r_s}{r_e}\right)^{-1+\xi_1} - \sigma_0\left(1-\frac{\xi_1}{\xi_2}\right)\left(\frac{r_s}{r_e}\right)^{-1-\xi_1}\right]$$

$$d_2 = \frac{r_s^{1+\xi_2}}{2}\left[\sigma_0 - \frac{\sigma_0}{\xi_2} - \sigma_0\left(1-\frac{\xi_1}{\xi_2}\right)\left(\frac{r_s}{r_e}\right)^{1+\xi_1} - \sigma_0\left(1+\frac{\xi_1}{\xi_2}\right)\left(\frac{r_s}{r_e}\right)^{1-\xi_1}\right]. \tag{25}$$

From the above results one can show that the assumptions (6) hold in this case.

Finally, we can notice that σ_s/σ_0 is connected with r_s/r_e through the relation

$$\frac{\sigma_s}{\sigma_0} = \xi_1\left[-\left(\frac{r_s}{r_e}\right)^{-1+\xi_1} + \left(\frac{r_s}{r_e}\right)^{-1-\xi_1}\right] + 1. \tag{26}$$

A plot of this curve is shown in Fig. 4.

The general results derived so far can be represented in a single graph of σ_{rr} and $\sigma_{\theta\theta}$. This graph is shown in Fig. 5, for $\nu_0 = 0.25$, $E_T/E_0 = 0.25$, $E_s/E_0 = 0.534$. One can notice the change of slope in the $\sigma_{\theta\theta}$ distribution. This graph can be used in the following way. From the graph and for $\sigma_{rr} = -p_0$, we can determine a radius which will actually be the real r_0, and which will scale the rest of the dimensions.

4. HOLE UNDER INTERNAL TENSION

It is interesting to state the general solution for the case when there is an internal tension instead of compression on the hole boundary. Following arguments similar to those in Section 3, microcracks may develop normal to the radial directions (Fig. 6). Then, we may assume a unilateral constraint of the type

$$\sigma_{rr} > \sigma_{\theta\theta}$$
$$\sigma_{rr} > \sigma_0 \quad \text{for all} \quad r_0 \leqslant r_e. \tag{27}$$

The above assumptions indicate that

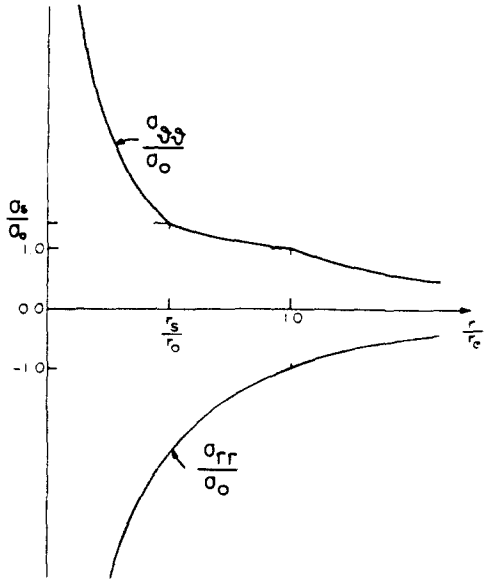

Fig. 5. Stress distributions σ_{rr}/σ_0 and $\sigma_{\vartheta\vartheta}/\sigma_0$ for a hole under internal pressure ($\nu_0 = 0.25$, $E_T/E_0 = 0.25$, $E_s/E_0 = 0.534$, $\sigma_s/\sigma_0 = 1.410$, $r_s/r_e = 0.6$).

$$\sigma_1 = \sigma_{rr}$$

$$\mathbf{n} = \begin{pmatrix} n_r \\ n_\vartheta \end{pmatrix} = \begin{pmatrix} 1 \\ 0 \end{pmatrix}. \tag{28}$$

Following an analysis similar to the one in Section 3, we may state the ordinary differential equation which controls the solution in the form

$$\lambda X = A(3rX_{,r} + r^2 X_{,rr}) \tag{29}$$

with

$$\lambda = \begin{cases} 0; & \sigma_{rr} \leqslant \sigma_0 \\ \left(C - \dfrac{\sigma_0 C}{X}\right); & \sigma_0 \leqslant \sigma_{rr} \leqslant \sigma_s \\ D; & \sigma_s \leqslant \sigma_{rr}. \end{cases} \tag{30}$$

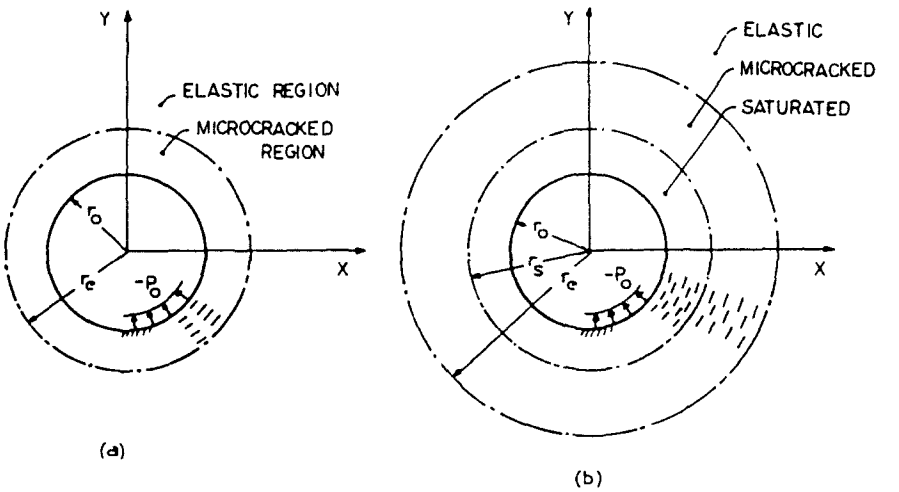

Fig. 6. The possible elastodamage boundaries for a hole under internal tension. (a) $\sigma_0 \leqslant p_0 \leqslant \sigma_s$. (b) $\sigma_s < p_0$.

The solution to (29) can be written for the three separate regions as was done in Section 3. The result is

$$X = l_1^{\mathrm{I}} r^{-2} + l_2^{\mathrm{I}}; \quad \sigma_{rr} \leqslant \sigma_0 \tag{31a}$$

$$X = l_1^{\mathrm{II}} r^{-1+\eta_1} + l_2^{\mathrm{II}} r^{-1-\eta_1} + \sigma_0; \quad \sigma_0 \leqslant \sigma_{rr} \leqslant \sigma_s \tag{31b}$$

$$X = l_1^{\mathrm{III}} r^{-1+\eta_2} + l_2^{\mathrm{III}} r^{-1-\eta_2}; \quad \sigma_s \leqslant \sigma_{rr} \tag{31c}$$

$$\eta_1 = \left(\frac{A+C}{A}\right)^{1/2} \tag{31d}$$

$$\eta_2 = \left(\frac{A+D}{A}\right)^{1/2}. \tag{31e}$$

The elastic solution would be

$$\sigma_{rr}(r \geqslant r_e) = \sigma_0 \left(\frac{r_e}{r}\right)^2$$

$$\sigma_{\theta\theta}(r \geqslant r_e) = -\sigma_0 \left(\frac{r_e}{r}\right)^2. \tag{32}$$

In the transition region the solution is

$$\sigma_{rr}(r_s \leqslant r \leqslant r_e) = l_1 r^{-1+\eta_1} + l_2 r^{-1-\eta_1} + \sigma_0$$
$$\sigma_{\theta\theta}(r_s \leqslant r \leqslant r_e) = \eta_1 (l_1 r^{-1+\eta_1} - l_2 r^{-1-\eta_1}) + \sigma_0. \tag{33}$$

In the saturation region the stresses are

$$\sigma_{rr}(r_0 \leqslant r \leqslant r_s) = f_1 r^{-1+\eta_2} + f_2 r^{-1-\eta_1}$$
$$\sigma_{\theta\theta}(r_0 \leqslant r \leqslant r_s) = \eta_2 (f_1 r^{-1+\eta_2} - f_2 r^{-1-\eta_2}). \tag{34}$$

The coefficients l_1 and l_2 can be determined from the continuity of tractions between the elastic and the transition distributions of stresses. The result is

$$l_1 = -\sigma_0 r_e^{1-\eta_1}/\eta_1$$
$$l_2 = \sigma_0 r_e^{1+\eta_1}/\eta_1. \tag{35}$$

The coefficients f_1 and f_2 can be determined from continuity of stresses between the transition and the saturation distributions of stresses. The result is

$$f_1 = \frac{r_s^{1-\eta_2}}{2}\left[\sigma_0 + \frac{\sigma_0}{\eta_2} - \frac{\sigma_0}{\eta_1}\left(1+\frac{\eta_1}{\eta_2}\right)\left(\frac{r_s}{r_e}\right)^{-1+\eta_1} + \frac{\sigma_0}{\eta_1}\left(1-\frac{\eta_1}{\eta_2}\right)\left(\frac{r_s}{r_e}\right)^{-1-\eta_1}\right]$$

$$f_2 = \frac{r_s^{1+\eta_2}}{2}\left[\sigma_0 - \frac{\sigma_0}{\eta_2} - \frac{\sigma_0}{\eta_1}\left(1-\frac{\eta_1}{\eta_2}\right)\left(\frac{r_s}{r_e}\right)^{-1+\eta_1} + \frac{\sigma_0}{\eta_1}\left(1+\frac{\eta_1}{\eta_2}\right)\left(\frac{r_s}{r_e}\right)^{-1-\eta_1}\right]. \tag{36}$$

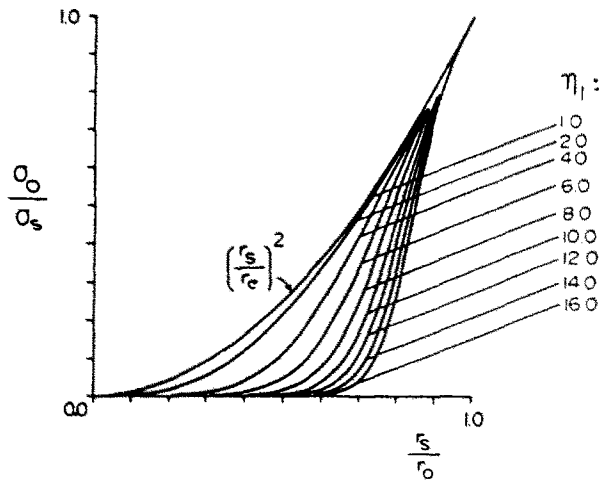

Fig. 7. The dependence of r_s/r_e on σ_0/σ, for a hole under internal tension ($\eta_1 = 1/\xi_1$, $\eta_1 \geq 1$).

One can also verify that the assumption (27) holds. Finally, we can again notice that σ_s/σ_0 is connected with r_s/r_e through the relation

$$\frac{\sigma_s}{\sigma_0} = \frac{1}{\eta_1}\left[-\left(\frac{r_s}{r_e}\right)^{-1+\eta_1} + \left(\frac{r_s}{r_e}\right)^{1-\eta_1}\right] + 1. \tag{37}$$

A plot of this curve is shown in Fig. 7.

The general results are represented in a single graph of σ_{rr} and $\sigma_{\theta\theta}$, shown in Fig. 8, with $\nu_0 = 0.25$, $E_T/E_0 = 0.15$, $E_s/E_0 = 0.332$. Note that the slope of the curves are continuous. The interpretation of the graph is that the stress level $\sigma_{rr} = p_0$, determines the radius which will be the real r_0, and which will scale the rest of the dimensions.

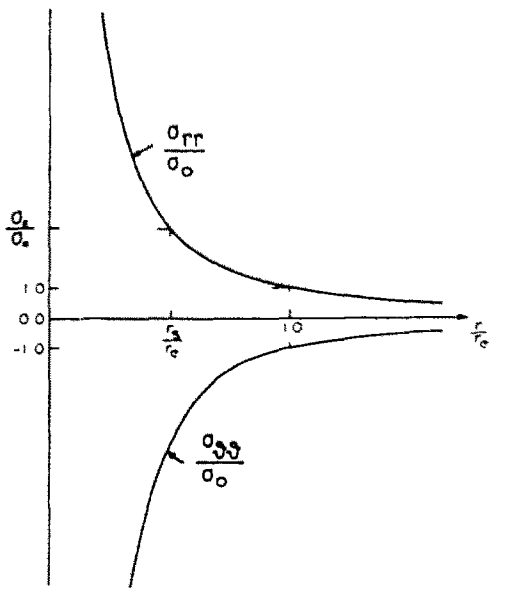

Fig. 8. Stress distributions σ_{rr}/σ_0 and $\sigma_{\theta\theta}/\sigma_0$ for a hole under internal tension ($\nu_0 = 0.25$, $E_T/E_0 = 0.25$, $E_s/E_0 = 0.332$, $\sigma_s/\sigma_0 = 3.031$, $r_s/r_e = 0.6$).

5. CONCLUSIONS

The results presented provide an exact solution for the axially symmetric ring problems when the material behaves as an anisotropically microcracking solid. These results can serve as the theoretical background for pressurized ring experiments evaluating the material constants involved in this type of constitutive laws. Furthermore, the results can be used for the structural analysis of ring-type components, made from ceramics. Finally, the analytic solution may form a basis for checking finite element algorithms that compute anisotropic damage.

There are few analytical solutions and test configurations that enable progressing microcracking to be developed in a confined way. The present paper deals with an axisymmetric case that makes possible the formation of stable damage. The particular case dealt with is suitable for confining the microcracked region in a controllable manner. This makes the ring geometry under internal pressure an attractive experimental configuration for ceramic materials. The additional fact that the microcracked region is confined is a very useful experimental asset because it makes the ring test much less sensitive to parasitic stresses which are present in uniaxial tests. Experiments on such ring specimens made of alumina are currently under way and we will present them in future publications.

A particular constitutive law for nontransforming ceramic materials has been used in the present analysis. This is a necessary simplification at present, since the constitutive identification of these materials is in its early stage, very similar to that of plasticity years ago. The constitutive law used in the present work takes into account the anisotropic damage and in particular the microcracks that are developed normal to the maximum tensile stress. This behavior has been observed in many nontransforming ceramics. The proposed constitutive model, although simple, includes the main features of the micromechanisms responsible for the overall mechanical behavior of such materials. It can also be shown that for the particular problem the strains are proportional. This fact makes the analysis valid even in the case where the strains are replaced by strain rates.

Studies on stress-induced microcracking have very useful applications. In particular, microcracking around a crack-tip may shield the tip from remote loads and enhance the toughness. Hence, in order to predict the increase in toughness, the material behavior needs to be quantified independently. The present solution can be used in structural applications such as pipes under internal pressure, and as a standard biaxial test for strength of ceramics. Other types of damage evolution function ($\lambda(\sigma_1)$) can also be used in expense of simplicity and numerical effort.

REFERENCES

Fu, Y. (1983). Mechanics of microcrack toughening in ceramics. Doctoral Dissertation, University of California at Berkeley.

Ortiz, M. (1987). A continuum theory of crack shielding in ceramics. *J. Appl. Mech.* **54**, 54.

Ortiz, M. and Giannakopoulos, A. E. (1989). Maximal crack-tip shielding by microcracking. *J. Appl. Mech.* **56**, 279.